Environmental Earth Sciences (2019) 78:2
https://doi.org/10.1007/s12665-018-7991-4

THEMATIC ISSUE

Patagonian salt marsh soils and oxidizable pedogenic pyrite: solid phases controlling aluminum and iron contents in acidic soil solutions

Pablo José Bouza[1] · Ileana Ríos[1] · Yanina Lorena Idaszkin[1,2] · Alejandro Bortolus[1,3]

Received: 21 December 2017 / Accepted: 11 December 2018

Abstract

The sulfidic materials present in salt marshes could be oxidized forming sulfuric acid, increasing the toxic levels of both Al and Fe available to plants. The objectives of this study were: (a) to evaluate the mechanism of acid generation from the oxidation of sulfidic materials, and (b) to predict solid phases governing the dissolved Fe and Al concentrations in soils at low pH. The study was conducted in 14 soil profiles associated to eight salt marshes situated along the Atlantic coast of Patagonia. The potential acidity was estimated by the peroxide-oxidizable sulfuric acidity method (POSA). To predict the availability of Fe and Al at low pH, the solid phase equilibrium that governs the solubility of these elements through ion activity of the products was determined. The scanning electron microscopy analysis in sulfidic materials reveals the occurrence of framboidal pyrite. The relative variability of POSA at low pH values may indicate retention of sulfates by Al and Fe hydroxides, producing the formation of basic sulfates of iron and aluminum. At pH > 5.5, Fe^{2+} and Al^{3+} activities show an equilibrium with amorphous oxy-hydroxides of $Fe(OH)_3$ and gibbsite, respectively. As the pH begins to decline below 5.5, Fe^{2+} and Al^{3+} activities show an equilibrium with respect to soil–$Fe(OH)_3$ and $Al(OH)_3$ amorphous, respectively. While for more acidic conditions, the solid phase in predicting both Fe^{2+} and Al^{3+} activities was basic iron sulfate and jurbanite. The acidic soil solutions with pH < 3, Fe^{2+} and SO_4^{2-} activities show an equilibrium with goethite and melanterite, respectively. As a consequence of acid generation, phosphorus adsorption by aluminum and iron oxide minerals was detected.

Keywords Pyrite framboids · Sulfidic materials · Potential acid sulfate soils · Tidal salt marsh · Solid phase equilibrium

Introduction

Tidal salt marshes worldwide are commonly located in estuarine or other coastal areas exposed to tidal action, but protected enough for the installation of terrestrial plants (halophytes), having a source of sediment and fresh water (Adam 1990; Allen 2000). Salt marsh soils are continuously saturated in some part of the soil profile and can be periodically affected by both tidal flooding and waterlogging, thereby they do not show some soil profile development grade, thus being commonly included in Aquents Suborder (Soil Survey Staff 1999). The high salinity and reducing conditions present in these soils are propitious for the occurrence of sulfidic materials (Great Group of Sulfaquents). The sulfates in the seawater and ferric oxides or iron-bearing silicates provided from sediments, are biologically reduced to sulfides (Eqs. 1, 2). Anaerobic bacteria use the organic matter as their source of energy (Van Breemen 1982):

$$SO_4^{2-} + 2CH_2O + 2H^+ \rightarrow H_2S + 2CO_2 + H_2O \quad (1)$$

This article is a part of Topical Collection in Environmental Earth Sciences on IV RAGSU—Advances in Geochemistry of the Surface in Argentina, edited by Dr. Americo Iadran Torres and Dr. Pablo Jose Bouza.

✉ Pablo José Bouza
bouza@cenpat-conicet.gob.ar

[1] Instituto Patagónico para el Estudio de los Ecosistemas Continentales (IPEEC), Centro Nacional Patagónico, CONICET, Boulevard Brown 2915, CP 9120 Puerto Madryn, Chubut, Argentina

[2] Universidad Nacional de la Patagonia San Juan Bosco, Boulevard Brown 3051, U9120ACD Puerto Madryn, Chubut, Argentina

[3] Grupo de Ecología en Ambientes Costeros (GEAC IPEEC-CONICET), Chubut, Argentina

Published online: 19 December 2018

$$2Fe_2O_3 + CH_2O + 8H^+ \rightarrow Fe^{2+} + CO_2 + 5H_2O \quad (2)$$

The main end product is pyrite (Eq. 3), although iron monosulfides and hydrogen sulfide gas can be formed as precursors (Ahern et al. 2004):

$$Fe_2O_3(s) + 4SO_4^{2-} + 8CH_2O + 1/2\ O_2 \rightarrow 2FeS_2(\text{pyrite}) + 8HCO^-_3 + 4H_2O \quad (3)$$

The soluble bicarbonate is removed from the sediments during the tidal flows, leaving accumulated sulfides as a source of potential acidity when these sediments are drained (White et al. 1997).

When these soils are drained, the sulfidic materials are oxidized forming sulfuric acid producing a drop in the pH (< 3.5). The complete oxidation and hydrolysis of iron to ferric hydroxide yields two moles of sulfuric acid per mole of pyrite (Eq. 4):

$$FeS_2 + 15/4\ O_2 + 7/2\ H_2O \rightarrow Fe(OH)_3 + 2SO_4^{2-} + 4H^+ \quad (4)$$

This oxidation processes is low, but the reaction rate is enhanced by the chemoautotrophic organism *Thiobacillus ferrooxidans*, in such a way that pyrite is oxidized more rapidly by Fe^{3+} than by oxygen (Van Breemen 1982) (Eq. 5):

$$FeS_2 + 14\ Fe^{3+} + 8\ H_2O \rightarrow 15\ Fe^{2+} + 16\ H^+ + 2SO_4^{2-} \quad (5)$$

The presence of carbonates and/or an elevated cation-exchange capacity (CEC) would help to neutralize this acidification process (Lin et al. 1996; Ahern et al. 2004). The CEC is provided either by the quantity and type of dominant clay minerals (Dent 1986) or by the quality and the decomposition degree of organic matter content (Sposito 1989; Haynes 2014). The CEC variation with clay mineral is due to a combination of ionic substitution (degree of cationic hydration) and the number of exchange sites at the clay lattice (Sposito et al. 1999). The 2:1 type clay minerals with outer-sphere surface complexes (hydrated cations, e.g., smectite and vermiculite) have great values of CEC than the 2:1 type clay with inner-sphere surface complex (dehydrated cations, e.g., illite) and 1:1 type clay minerals (e.g., kaolinite). The high CEC of organic matter is attributed mainly both to humic acids (carboxylic and phenolic radicals; Stevenson 1994) and humin fractions (Yagui et al. 2003).

This acidic soil condition limits plants' growth by increasing the toxic levels of both Al and Fe available in the soil solution (Dent 1986). To predict the availability of Fe and Al to plants, it is important to determine the potential solid phase governing the solubilities of these elements at low pH environments (Reddy et al. 1995). Generally the understanding of these relationships—unlike salt marsh environment—is well-known in areas with soil disturbance by pyritic coal surface mining (Devasahayam 2006), polysulfide ore deposits (Sullivan et al. 1988a, b; Ludwig et al. 2001) or sedimentary rocks of lacustrine-swampy environments (Reddy et al. 1995).

The salt marshes of the Argentine Patagonian region in southern South America (40°S–55°S latitude; Soriano 1983) have received little attention from scientists (Bortolus and Schwindt 2007). This is probably because the Patagonian coast region is devoid of great coastal plains, like those in the northern coast of Argentina (i.e., Buenos Aires province) or in the Atlantic and Gulf of Mexico coasts of North America. However, the Patagonian large tidal ranges (up to ~ 14 m of amplitude) often combine with gently sloped terrains to produce areas with muddy marine sediments protected from wave action and lead to the formation of salt marshes. In fact, a large-scale survey confirmed the occurrence of several heretofore unknown salt marshes in many locations along the Patagonian coast (Bortolus et al. 2009). In a preliminary study, soils of salt marshes on Argentine Patagonian coast have been characterized by Bouza et al. (2008), who identified the occurrence of sulfidic materials.

The objectives of this work were: (a) to evaluate the mechanism of acid generation from the oxidation of sulfidic materials and (b) to predict solid phases governing the dissolved Fe and Al concentrations in soils at low pH.

Study area

The study was conducted on 14 soils developed in salt marshes situated along the Atlantic coast of Patagonia from Caleta Los Loros Reserve (Río Negro province, 40°43′19″S, 64°51′39″W) to Río Gallegos city (51°37′23″S, 69°01′31″W; Fig. 1). *Spartina* marshes are more common and larger in the northern part of Patagonia (latitudes lower than 42°S), while *Sarcocornia* marshes at latitudes higher than 42°S (Table 1), and these two marsh physiognomies overlap between 42°S and 43°S (Bortolus et al. 2009).

The climate on the coasts of Río Negro, Chubut, and north Santa Cruz provinces is cold and dry with an important annual oscillation. The mean annual temperature (MAT) varies between 18 and 12 °C (January can vary between 22 and 12 °C, and July between 10 and 2 °C). Southwards, the MAT decreases considerably. The mean annual precipitation (MAP) reaches values between 300 and 200 mm, while the mean annual evapotranspiration (MAE) values vary between 500 and 600 mm, which mean that the region has a strong annual water deficit. On the other hand, the climate on the southern Santa Cruz province coast is arid and cold. The MAT varies between 12 and 6 °C, with winter month close to 0 °C (July). The MAP varies between 400 and 200 mm, decreasing sharply in a west–east direction. The tidal ranges of the studied salt marshes are macro-tidal

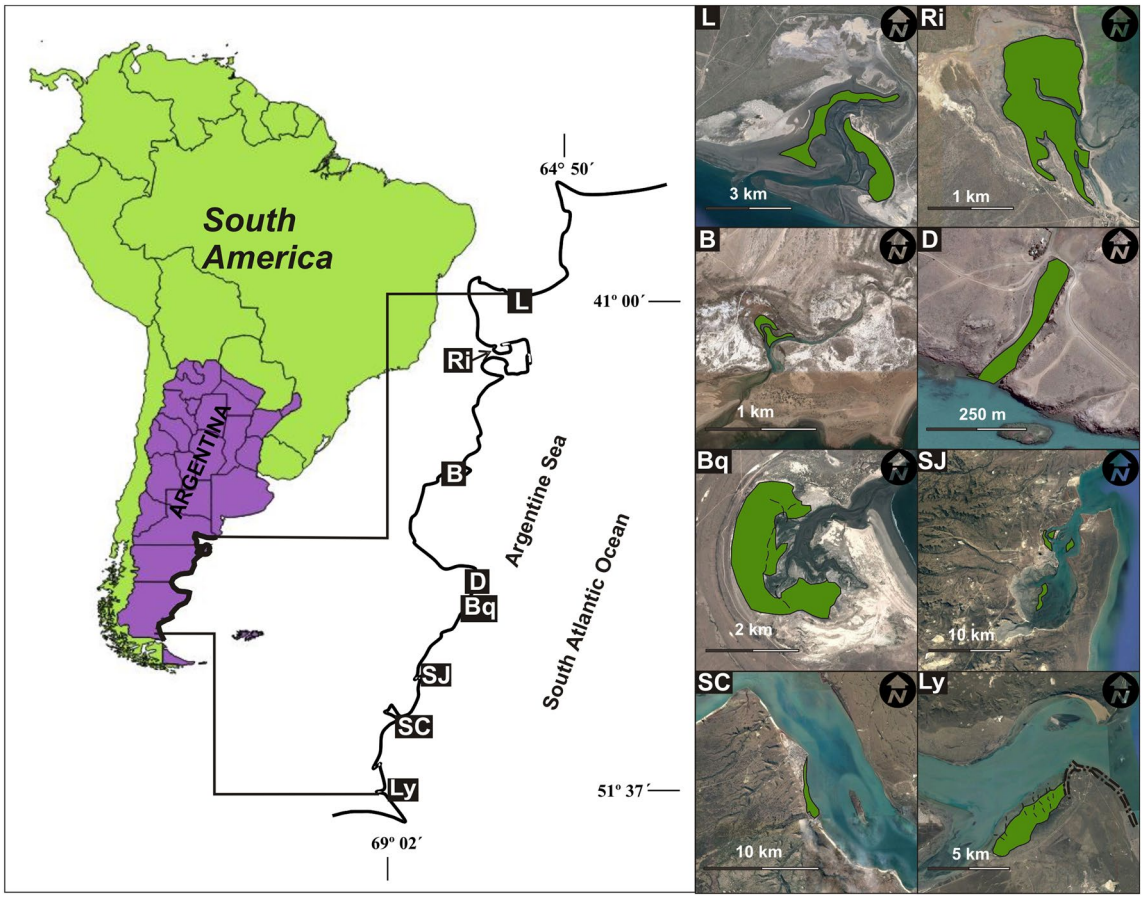

Fig. 1 Location of the salt marshes studied (green areas). L, Loros; Ri, Riacho; B, Bustamante; D, Deseado; Bq, Buque; SJ, San Julián; SC, Santa Cruz; Ly, Loyola

Table 1 Locations, climatic conditions, dominant vegetation, and tide mean amplitudes of the tidal salt marshes studied

Marshes	Location		MAT (°C)	MAP (mm year^{-1})	MAE (mm year^{-1})	AI	TMA (m)	Dominant vegetation
	Lat. (-S)	Long. (-W)						
Loros[a]	41°00′07″	62°47′23″	15.1	243	1165	0.21	6.04	SP
Riacho[b]	42°24′47″	64°37′21″	13.6	170	932	0.18	5.06	SP
Bustamante[c]	45°05′31″	66°30′31″	9.4	145	649	0.22	3.87	SA
Deseado	47°44′45″	65°56′50″	10.1	243	692	0.35	3.84	SA
Buque[d]	48°03′31″	65°59′22″	10.1	243	692	0.35	3.84	SA
San Julian	49°16′13″	67°43′31″	9.0	193	831	0.23	6.14	SA
Santa Cruz	50°01′26″	68°30′49″	8.5	200	800	0.25	8.05	SA
Loyola	51°37′23″	69°01′31″	6.9	222	918	0.24	8.27	SA

MAT, MAP and MAE: mean annual temperature, precipitation and evapotranspiration, respectively; AI, Aridity Index (UNEP 1997); Climate data of nearest localities

[a]San Antonio Oeste city (40°26′-S, 64°24′-W)

[b]Puerto Madryn city (42°65′-S, 65°03′-W)

[c]Camarones town (44°29′-S, 65°25′-W)

[d]Puerto Deseado. TMA, tide mean amplitude (SHN 2018); SP, *Spartina*-dominated marsh; SA, *Sarcocornia*-dominated marsh

type (> 4 m; Codignotto et al. 1993). Climatic conditions, tidal mean amplitudes and dominant plants for the study sites are shown in Table 1.

According to the geomorphological classification proposed by Allen (2000), Bouza et al. (2008) recognized three types of salt marshes on the Patagonian coast (Fig. 1) were: (1) estuarine salt marshes (e.g., Santa Cruz and Loyola marshes): these marshes are located in the mouth of the largest rivers, partially protected from the wave action by sand bars, the dominant sediment grain size in the intertidal plain is loam and clay loam; (2) open embayment (e.g., Loros marsh): with a sediment grain size predominantly sand; and (3) restricted-entrance embayment salt marsh (e.g., Riacho, Buque and San Julián marshes): characterized by a sandy-loam sediment grain size, and protected from the wave action by sandy and/or gravel spits (Bouza et al. 2008). The soil parent materials have a predominantly siliciclastic composition, although small amounts of shell fragments are observed. Some of the marshes we surveyed are embedded in a complex integrated by several salt marshes within the same estuary intermixed with other intertidal environments like mudflats, sandy beaches and rocky shores (Bortolus et al. 2009). Although Deseado marsh belongs to one of these salt marsh complexes, it is located within a small coastal valley cut on volcanic rocks and it is a clear example of a restricted-entrance embayment salt marsh (Fig. 1). Also, Bustamante marsh is protected from the wave action by a combination of volcanic rock outcrop and sandy spits located in the mouth of the main channel.

The studied soils have different redoximorphic features (Vepraskas et al. 1994) like redox concentration around macropores (as roots and rhizome), stratified sediments and nodules. These redox concentrations showed reddish brown colors (hue 5YR) presumably indicating the occurrence of ferrihydrite ($5Fe_2O_3{\cdot}9H_2O$) and environments subject to rapid oxidation of Fe^{2+} in presence of organic matter (Fitzpatrick and Shand 2008).

Table 2 shows the main soil properties from profiles performed in low and high marsh physiographic levels (Bouza et al. 2008), and soil classification at the Great Group taxa (Soil Survey Staff 1999).

Materials and methods

One soil pit (~ 1 m^2 surface area and ~ 1 m depth) was dug per marsh level within each salt marsh to describe the soil profiles, and then a soil sample (500 cm^3) from each soil horizon was collected from the different marsh levels. The low (L) and high (H) marsh levels were defined as the lower and upper half of the elevation gradient within each physiographic site (status and type of vegetation). The morphological descriptions and classification of the soils were conducted following the procedures of Schoeneberger et al. (2012) and Soil Survey Staff (1999), respectively. All soil horizon samples were zip-locked and taken to the laboratory in hermetic containers (kept at ~ 4 °C during transport to laboratory, and then they were stored in freezer to ~ − 20 °C) to perform the remaining physicochemical analyses. All samples were collected during winter months with the aim to preserve the soil samples at lowest possible temperature.

To determine the presence of sulfidic materials (Soil Survey Staff 1999), incubation soil pH was measured once a week till stabilization, putting the soils under moist aerobic conditions (1-cm-thick layer at field capacity) at room temperature. The presence of sulfidic material (oxidizable sulfur compounds) used as criterion for soil classification (Sulfaquents) occurs when there is a drop in pH from 0.5 or more units to a pH value of 4.0 or less (1:1) by weight in water or in a minimum of water to permit measurement within 8 weeks.

After 24 h oven-drying at 85 °C to destroy sulfide-oxidizing bacteria, soil subsamples were screened through 2 mm mesh (Lin et al. 1996).

For selected subsamples < 2 mm, the SO_4^{2-} concentration, pH, Eh and electrical conductivity (EC) were measured from two extracts: (1) 1:2.5 initial soil/water extract (w) and (2) 1:2.5 soil/water extract, previously treated with hydrogen peroxide 30% (p). The sulfate contents in both extracts were determined by the electroconductometric method (US Salinity Laboratory Staff 1954). The pyrite-derived potential acidity was estimated by peroxide-oxidizable sulfuric acidity (POSA), which indicates the potential acidity from sulfuric acid generation after oxidation of inorganic sulfides with hydrogen peroxide treatment (Lin and Melville 1993, 1994; Lin et al. 1995). The POSA method was defined by Lin and Melville (1993) as:

$$\text{POSA}\left(\text{cmol}_c\ \text{kg}^{-1}\ \text{soil}\right) = \left({SO_4}^{2-}{}_p - {SO_4}^{2-}{}_w\right) \cdot 2$$

The POSA method was selected in this study due to (1) the relative low contents of organic matter, thus the possible interference by sulfides from organic matter is minimum, and (2) the absence of sulfate minerals as gypsum and jarosite commonly found in acid sulfate soils (Sullivan et al. 1999; Ahern et al. 1998). On the other hand, the POSA parameter was satisfactory used for the purpose of acid sulfate soil–landscape studies, which mainly require comparison of the relative quantity of potential sulfuric acidity through soil profile and landscape sequence (Lin and Melville 1994; Lin et al. 1995).

The contents of Fe and Al in oxidized soil solutions (p) were measured with an IL 457 atomic absorption spectrophotometer (Instrumentation Laboratory Incorporation Lexington, USA).

Table 2 Selected soil properties of the salt marshes studied (from Bouza et al. 2008)

Marshes' physiographic positions Soil classification	Horizon	Depth (cm)	Color	Sand (%)	Silt (%)	Clay (%)	pH	pHi	LOI (%)	EC (dSm^{-1})	$CaCO_3$ (%)	CEC ($cmol_{(c)}kg^{-1}$)
Loros, low	A	0–10	5Y 5/2	66.7	31.2	2.1	7.12	3.03	1.8	37.0	0.05	12.26
Sulfaquents	C1	10–20	5Y 5/2	74.3	21.5	4.1	7.96	3.16	0.9	35.8	0.49	13.57
	C2	> 20	5Y 4/2	91.6	6.3	2.1	8.37	3.90	1.3	27.3	0.13	7.30
Riacho, low	Ag	0–20	5Y 3/2	3.8	79.6	16.6	7.50	4.90	22.2	90.2	0.66	52.2
Sulfaquents	Bg1	20–44	5Y 3/2	4.3	79.2	16.5	7.20	3.50	24.7	92.0	0.62	52.2
	Bg2	44–64	5Y 3/2	2.3	79.7	18.0	7.30	5.40	25.2	117.1	0.51	52.2
	Cg	64–138	5Y 3/1	3.0	82.0	15.0	7.30	3.90	15.1	52.7	0.68	51.3
	2Cg	> 138	5Y 4/1	76.7	15.8	7.6	7.70	4.30	2.2	17.4	0.85	11.7
Bustamante, low	A1	0–5	5Y 5/3	29.1	39.5	31.4	6.85	6.62	8.3	39.4	0.19	38.26
Fluvaquents	A2	5–18	10YR 5/4	58.1	12.5	29.4	6.68	6.72	0.7	31.2	0.69	5.16
	Cg	> 18	5Y 4/3	56.1	25.5	18.3	7.05	6.19	5.6	64.2	0.25	45.48
Bustamante, high	A1	0–5	5 Y 5/3	6.3	24.4	69.3	7.97	8.27	12.8	nd	2.57	10.78
Fluvaquents	A2	5–40	10YR 5/4	82.5	7.2	10.3	7.21	7.18	1.8	31.1	0.56	45.39
	Cg	> 40	5Y 4/3	64.7	24.4	10.9	6.57	6.94	3.8	42.9	0.55	42.61
Deseado, low	Ag	0–16	5Y 5/3	1.0	68.3	31.7	6.26	6.48	14.1	64.3	2.49	27.30
Fluvaquents	Bg	16–21	2.5Y 4/0	83.7	5.4	10.9	6.98	7.17	4.0	42.7	1.81	35.30
	Cg	> 21	2.5Y 2/0	15.1	24.9	60.0	5.68	5.08	6.9	54.0	1.59	44.70
Deseado, high	A	0–2	10YR 4/4	57.8	15.7	26.5	7.77	8.27	5.8	7.3	1.05	21.39
Hydraquents	C1	2–17	10YR 4/3	60.0	11.5	28.5	7.48	8.08	3.6	18.3	1.09	21.39
	C2	> 17	10YR 4/3	72.5	7.3	20.2	7.46	7.94	2.6	27.0	0.72	17.13
Buque, low	A	0–24	5Y 5/3	59.0	27.9	13.1	7.15	6.90	4.0	37.7	0.75	13.30
Fluvaquents	Bg	24–27	5Y 4/2	36.4	51.6	11.9	7.03	7.02	1.7	45.3	1.16	4.45
	Cg1	27–50	10YR 4/3	91.1	0.0	8.9	7.82	8.03	0.8	63.6	4.25	4.97
	Cg2	> 50	5Y 5/2	26.1	40.6	33.3	6.86	4.42	3.3	71.9	3.95	23.83
Buque, high	A	0–3	5Y 5/3	65.8	20.9	13.3	7.22	nd	3.8	36.4	3.51	13.74
Fluvaquents	Bg	3–6	10YR 4/2	43.9	39.8	16.4	7.54	8.19	2.1	51.4	2.93	11.13
	C	6–46	5Y 4/2	84.7	11.6	3.7	7.66	7.96	1.0	64.2	3.45	6.50
	Cg	> 46	5Y 5/2	44.6	40.7	14.7	7.47	7.92	5.6	111.3	2.06	25.83
San Julian, low	A	0–19	5Y 4/3	0.5	89.2	10.4	6.94	7.46	3.4	33.6	0.52	20.35
Hydraquents	C1	19–32	5Y 4/3	21.3	68.2	10.5	6.51	7.32	3.3	39.4	0.59	24.70
	C2	> 32	5Y 4/2	28.7	50.0	21.3	6.19	6.56	3.2	63.8	0.17	25.13
San Julian, high	A	0–10	5Y 4/3	19.6	61.2	19.2	7.35	6.31	4.2	35.0	1.31	28.00
Hydraquents	Cg	> 10	5Y 4/6	19.3	55.2	25.5	7.00	7.89	3.7	27.7	0.30	31.04
Santa Cruz, low	A1	0–24	5Y 5/3	23.1	47.2	29.7	6.92	7.17	3.9	27.7	0.56	32.09

Table 2 (continued)

Marshes' physiographic positions Soil classification	Horizon	Depth (cm)	Color	Sand (%)	Silt (%)	Clay (%)	pH	pHi	LOI (%)	EC (dSm^{-1})	$CaCO_3$ (%)	CEC ($cmol_{(c)}kg^{-1}$)
Fluvaquents	A2	24–38	5Y 5/1	18.2	41.5	40.3	6.29	7.11	5.4	43.7	0.57	40.96
	Cg	> 38	5Y 4/1	26.3	42.1	31.7	7.06	6.36	3.5	45.1	0.25	28.70
Santa Cruz, high	A	0–4	5Y 4/2	18.5	47.1	34.4	7.18	7.05	5.2	28.5	0.78	31.48
Hydraquents	C1	4–34	5Y 4/2	32.9	32.7	34.4	6.60	7.96	3.2	60.5	0.15	31.74
	C2	34–64	5Y 5/2	42.7	22.7	34.6	6.35	6.61	3.6	76.3	0.35	31.48
	C3	> 64	5Y 4/1	37.3	27.9	34.8	6.56	6.39	3.6	71.5	0.13	25.83
Loyola, low	Ag1	0–15	5Y 5/3	18.1	47.3	34.6	6.63	6.68	2.8	36.0	0.42	24.43
Fluvaquents	Ag2	15–34	5Y 5/3	20.3	45.2	34.5	6.65	6.76	1.8	34.3	0.34	19.13
	2Cg	> 34	7.5YR 6/4	43.8	51.1	5.2	6.57	6.71	2.9	40.3	0.70	20.96
Loyola, high	A1	0–20	5Y 5/3	37.4	46.2	16.4	6.41	6.49	6.0	32.8	0.33	23.74
Hydraquents	C1	20–40	5Y 5/3	35.2	41.1	23.7	6.08	6.14	3.5	49.5	0.23	19.74
	C2	40–60	5Y 5/3	43.9	37.7	18.3	6.12	6.09	3.0	51.8	0.15	19.57
	Cg	> 60	5Y 5/3	65.8	20.9	13.3	7.24	7.19	2.0	45.9	0.49	16.87

EC, electrical conductivity; pH, initial pH (in situ); pHi, incubation pH (Soil Survey Staff 1999); LOI, loss organic ignition; CEC, cation-exchange capacity; nd, not determined

Table 3 Chemical reaction equilibrium

Reactions	log *K*
$Fe(OH)_{3\ amorphous} + 3H^+ = Fe^{3+} + 3H_2O$	4.89
$Fe^{3+} + e^- = Fe^{2+}$	13.04
$Fe(OH)_{3\ amorphous} + 3H^+ + e^- = Fe^{2+} + 3H_2O$	**17.93**
$Fe(OH)_{3\ soil} + 3H^+ = Fe^{3+} + 3H_2O$	2.70
$Fe^{3+} + e^- = Fe^{2+}$	13.04
$Fe(OH)_{3\ soil} + 3H^+ + e^- = Fe^{2+} + 3H_2O$	**15.74**
$\alpha\text{-}FeOOH_{\ goethite} + 3H^+ = Fe^{3+} + 2H_2O$	− 0.02
$Fe^{3+} + e^- = Fe^{2+}$	13.04
$\alpha\text{-}FeOOH_{\ goethite} + 3H^+ + e^- = Fe^{2+} + 2H_2O$	**13.02**
$FeOHSO_{4\ basic\ ferric\ sulfate} = Fe^{3+} + OH^- + SO_4^{2-}$	− 24.06
$Fe^{3+} + e^- = Fe^{2+}$	13.04
$OH^- + H^+ = H_2O$	14.00
$FeOHSO_{4\ basic\ ferric\ sulfate} + e^- + H^+ = Fe^{2+} + SO_4^{2-} + H_2O$	**2.98**
$FeSO_4{\cdot}7H_20_{\ melanterite} = Fe^{2+} + SO_4^{2-} + 7\ H_2O$	**− 4.66**
$Al(OH)_{3\ gibbsite} + 3H^+ = Al^{3+} + 3H_2O$	**8.11**
$Al(OH)_{3\ amorphous} + 3H^+ = Al^{3+} + 3H_2O$	**10.80**
$AlOHSO_{4\ basic\ aluminum\ sulfate}{}^* = Al^{3+} + OH^- + SO_4^{2-}$	− 17.23
$OH^- + H^+ = H_2O$	14.00
$AlOHSO_{4\ basic\ aluminum\ sulfate} + H^+ = Al^{3+} + SO_4^{2-} + H_2O$	**− 3.23**

The ionic activities were calculated according to Davies´s equation (Lindsay 1979), where the ionic strength was estimated from EC values (Griffin and Jurinak 1973).

The equilibrium constants (K°), used for solid phase equilibrium, were taken from Van Breemen (1973) and Lindsay (1979). The equilibrium constants of possible solid phases were calculated from the reactions given in Table 3.

The basic aluminum sulfate ($AlOHSO_4$) and jurbanite ($AlOHSO_4{\cdot}5H_2O$) have a similar solid phase equilibrium (K° are − 17.23 and − 17.80, respectively). The equilibrium constant of basic aluminum sulfate was used in this study, which was taken from Van Breemen (1973). Soil–$Fe(OH)_3$ is used as reference solid phase controlling the solubility for Fe^{3+} in soils (Lindsay 1979). The solubilities of hematite and goethite are nearly identical (log K° are 0.09 and − 0.02, respectively), but as goethite is considered the ultimate weathering product of iron in soil environment (Lindsay 1979), this oxide was used for graphical analysis.

To predict the availability of Fe and Al to plants at low pH, the solid phase equilibrium governing the solubility of these elements was determined. These solubilities were evaluated through ionic activity product (IAP) of the most probable minerals (IAP = K°: solid phase–soil solution equilibria; IAP < K°: solid phase dissolution; IAP > K°: solid phase precipitation; Sposito 1989).

On the same soil samples, a Jeol JSM 6460 LV scanning electron microscope (SEM) with an EDAX PW7757/78 energy-dispersive X-ray spectroscopy analyzer (EDS) and a Zeiss Supra 40 scanning electron microscope with EDS

Oxford Instruments were used to examine the morphology of sulfidic and oxidized materials and to determine the composition of certain soil particles.

Results

The SEM analysis in selected soil horizons with sulfidic materials revealed the occurrence of framboidal pyrite (from French word: *framboise*, raspberry patterns; Fig. 2), varying in diameter from 3 to 35 µm. Loros marsh had a predominately sandy texture and low organic matter content (Table 1). In C2 horizon, pyrite framboids were frequent and occurred as spheroidal aggregates of octahedral pyrite microcrystals, which reached from 0.2 to 2 µm (Fig. 2a, b). On the other hand, Riacho marsh had a predominately silt loam texture, had similar framboids to Loros marsh, but there were also numerous isolated, twinned and intergrown octahedral microcrystals (Fig. 2c). The EDS analysis showed the S:Fe atomic ratio (2:1) indicating the pyrite formula (Fig. 2d). Other secondary peaks in the energy-dispersive spectra as Si, Al and Na were identified.

The soil properties to characterize the acid generation and Fe and Al contents in oxidized solutions are summarized in Table 4. Comparing the soil properties shown in Table 2, in some marsh soil horizons, the incubation pH did not decrease during aerobic oxidation, while both initial and incubation pH values dropped drastically (below 3 or ΔpH greater than 2) after hydrogen peroxide treatment (e.g., Cg horizons of Bustamante low, Deseado low and Buque marshes), indicating the presence of pyrite and therefore the occurrence of potential acid sulfate soils (Ahern et al. 1998; Alsemgeest et al. 2005).

Figure 3 shows the framboidal pyrite from Cg2 horizon of Buque marsh after aerobic incubation. The micro-crystal aggregates analyzed in the SEM and EDS spectrum showed aluminum–iron–silicon coatings on framboidal pyrites, indicating the delay effect on aerobic oxidation.

Figure. 4 shows the relationship between ΔpH versus POSA and Eh_p, indicating that this acid generation after hydrogen peroxide treatment could be caused by pyrite

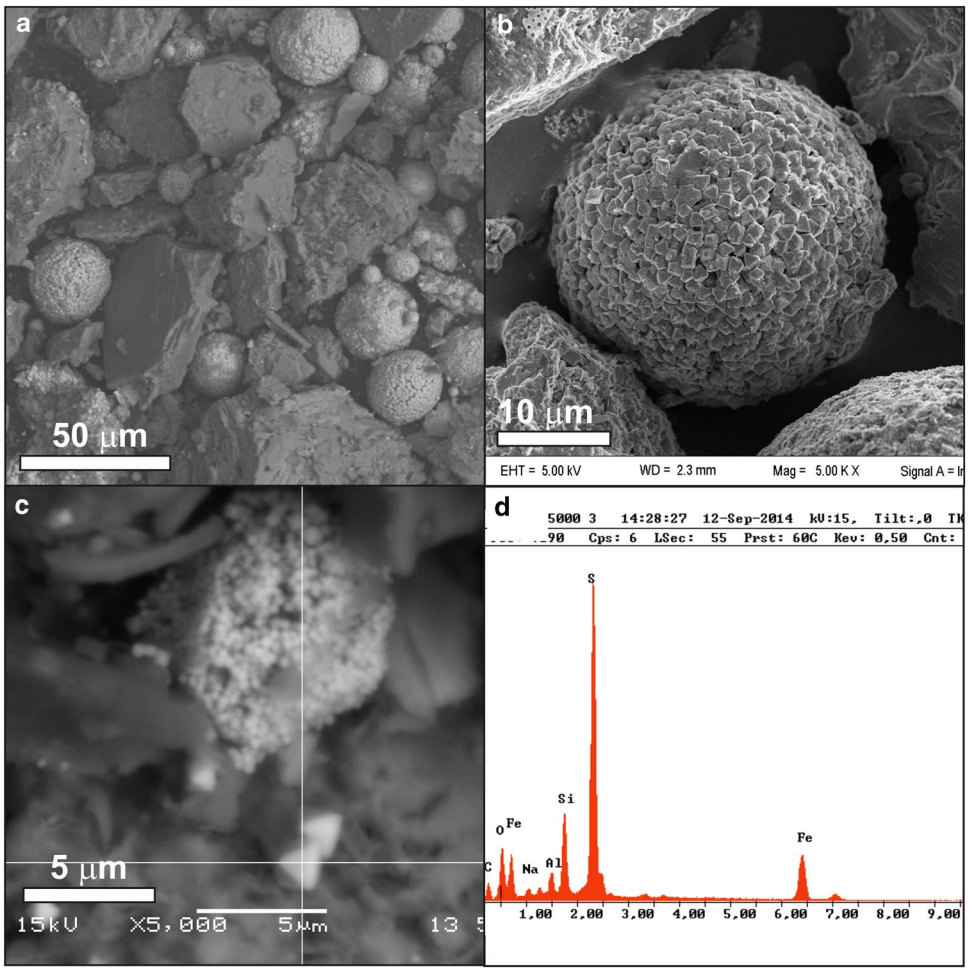

Fig. 2 **a** Framboidal pyrites of different size from Loros marsh; **b** details of both framboidal pyrite and octahedral habit pyrite in framboid; **c** microcrystals of octahedral pyrite (twinned crystal) from Riacho marsh; **d** EDS spectrum on octahedral pyrite

Table 4 Chemical properties of the soil solutions oxidized

Marshes physiographic positions	Horizon	pH_w	pH_p	ΔpH	Eh_p	pe_p	pe_p+pH_p	CE_p	$CaSO_{4\,w}$	$CaSO_{4\,p}$	Fe	Al
Soil classification		(1:2.5)	(1:2.5)		(mV)			(dSm^{-1})	($cmol_c\ kg^{-1}$)	($cmol_c\ kg^{-1}$)	(ppm)	(ppm)
Loros, low	A	6.98	3.31	3.7	491	8.30	11.61	6.86	7.71	13.10	10.90	91.30
Sulfaquents	C1	6.53	2.70	3.8	528	8.92	11.62	8.34	9.97	18.44	141.00	269.00
	C2	6.64	2.59	4.1	562	9.50	12.09	7.88	4.89	17.11	254.00	245.00
Riacho, low	Ag	6.36	2.43	3.9	524	8.86	11.28	10.55	9.24	19.61	44.60	28.30
Sulfaquents	Bg	5.85	1.86	4.0	548	9.26	11.12	12.48	2.08	17.49	101.40	283.40
	Bg2	6.70	1.94	4.8	563	9.51	11.45	13.84	3.11	18.13	74.30	203.70
	Cg	6.13	2.14	4.0	503	8.50	10.64	10.48	15.71	22.55	71.90	387.70
	2Cg	6.98	2.67	4.3	539	9.11	11.78	2.89	3.10	9.52	13.00	11.80
Bustamante, low	A1	6.97	6.91	0.1	247	4.17	11.08	8.87	4.90	4.81	1.40	bd
Fluvaquents	A2	6.85	6.61	0.2	284	4.80	11.41	5.14	0.12	1.15	bd	bd
	Cg	8.02	3.80	4.2	432	7.30	11.10	17.74	5.29	15.40	30.70	90.70
Bustamante, high	A1	8.83	7.34	1.5	200	3.38	10.72	2.13	0.00	4.19	nd	nd
Fluvaquents	A2	7.60	6.50	1.1	268	4.53	11.03	3.63	0.00	0.24	nd	nd
	Cg	6.90	6.13	0.8	254	4.29	10.42	8.67	2.38	6.30	nd	nd
Deseado, low	Ag	7.22	6.28	0.9	247	4.44	10.72	10.65	3.70	11.10	nd	nd
Fluvaquents	Bg	7.93	6.48	1.5	284	4.02	10.50	7.89	3.57	11.38	nd	nd
	Cg	7.93	5.07	2.9	432	5.02	10.09	9.46	4.23	19.56	nd	nd
Deseado, high	A	8.36	6.98	1.4	200	4.06	11.04	1.81	0.00	4.75	nd	nd
Hydraquents	C1	7.86	6.69	1.2	268	3.95	10.64	3.63	0.00	3.20	nd	nd
	C2	7.82	7.28	0.5	254	3.11	10.39	5.75	0.00	2.14	nd	nd
Buque, low	A	7.20	6.62	0.6	273	4.61	11.23	8.87	1.32	5.20	0.07	bd
Fluvaquents	Bg	7.59	7.31	0.3	257	4.34	11.65	9.75	3.17	3.76	bd	bd
	Cg1	8.51	8.05	0.5	250	4.23	12.28	7.98	1.78	1.80	bd	bd
	Cg2	7.57	3.01	4.6	506	8.55	11.56	19.39	8.74	28.50	34.00	326.00
Buque, high	A	8.36	7.34	1.02	180	3.04	10.38	10.91	0.23	8.42	0.14	bd
Fluvaquents	Bg	8.41	7.42	0.99	170	2.87	10.29	9.91	0.00	4.61	0.09	bd
	C	8.65	7.83	0.82	238	4.02	11.85	6.98	1.54	2.10	0.09	bd
	Cg	7.36	3.09	4.27	332	5.61	8.70	29.09	12.79	29.86	841	273.00
San Julian, low	A	7.40	5.64	1.8	250	4.23	9.87	10.67	0.00	6.06	10.50	0.74
Hydraquents	C1	6.67	5.46	1.2	323	5.46	10.92	11.64	1.54	4.15	26.00	30.30
	C2	6.70	5.27	1.4	381	6.44	11.71	12.61	2.85	5.79	2.65	8.37
San Julian, high	A	8.40	6.68	1.7	240	4.06	10.74	9.70	0.00	4.56	0.18	bd
Hydraquents	Cg	7.40	5.85	1.6	219	3.70	9.55	7.97	0.00	4.29	6.14	22.60
Santa Cruz, low	A1	6.99	5.44	1.6	258	4.36	9.80	7.60	0.00	4.42	nd	nd
Fluvaquents	A2	6.76	5.47	1.3	257	4.34	9.81	8.99	0.76	3.37	nd	nd
	Cg	7.69	6.20	1.5	239	4.04	10.24	12.05	1.93	5.20	nd	nd
Santa Cruz, high	A	7.84	6.08	1.8	230	3.89	9.97	9.27	0.00	6.25	nd	nd
Hydraquents	C1	6.95	5.77	1.2	250	4.23	10.00	14.83	2.59	5.46	nd	nd
	C2	6.87	6.52	0.4	213	3.60	10.12	13.91	2.51	5.08	nd	nd
	C3	6.98	6.45	0.5	215	3.63	10.08	12.05	1.05	4.82	nd	nd
Loyola, low	Ag1	7.15	6.20	1.0	255	4.31	10.51	9.70	1.72	4.42	0.15	bd
Fluvaquents	Ag2	7.17	6.71	0.5	231	3.90	10.61	7.37	1.05	1.55	bd	bd
Loyola, high	A1	6.49	5.62	0.9	288	4.87	10.49	10.67	0.79	1.55	164.00	125.00
Hydraquents	C1	6.41	5.81	0.6	298	5.04	10.85	11.64	3.04	3.74	23.00	22.06
	C2	6.50	5.98	0.5	220	3.72	9.70	10.91	1.98	3.06	1.28	0.42
	Cg	7.90	7.02	0.9	219	3.70	10.72	8.92	1.05	3.20	bd	bd

nd, not determined; bd, below detection limit (Fe < 0.05 ppm, Al < 0.2 ppm); $pe_p = 16.9\ Eh_p(V)$

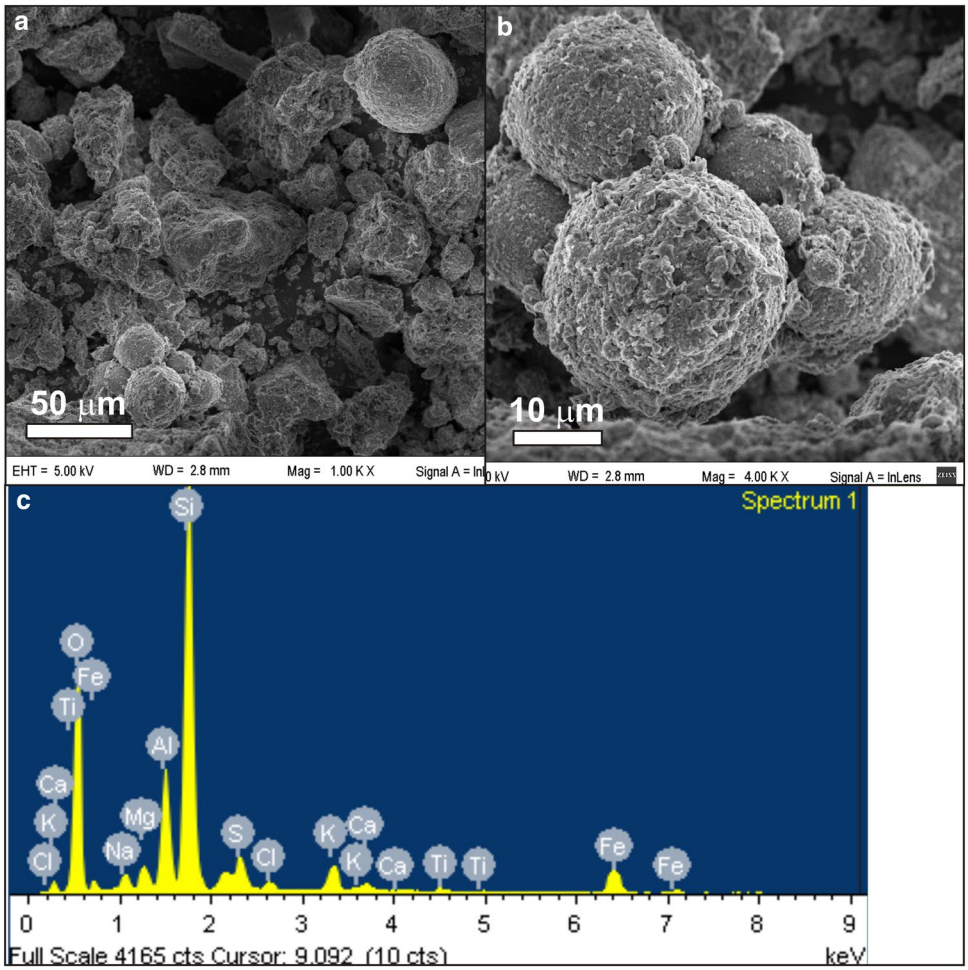

Fig. 3 **a** Framboidal pyrites from Cg2 horizon of Buque marsh after aerobic incubation; **b** EDS spectrum shows the occurrence of aluminum–iron–silicon coatings on framboidal pyrites

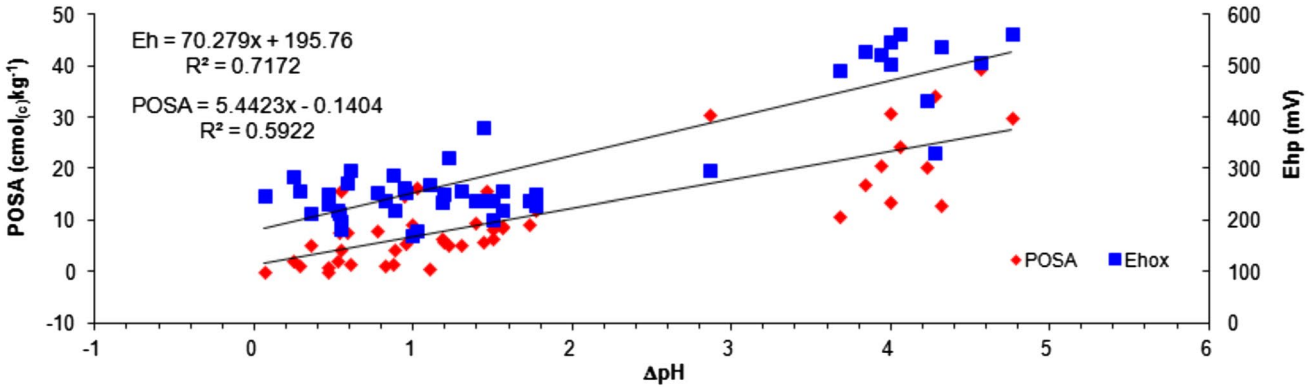

Fig. 4 Relationship between ΔpH versus POSA and Eh_p

oxidation. Also, a relative variability of POSA at low pH_p was observed.

According to the iron redox environment, redox reactions and Fe^{2+} solubility (Table 3) can be expressed as log Fe^{2+}/Fe^{3+}=13.04–pe (− log of electron activity). When pe = 13.04 the ratio of Fe^{2+}/Fe^{3+} is unity. Changing pe by one unit increases the ratio Fe^{2+}/Fe^{3+} 10-fold. Thus, the ratio Fe^{2+}/Fe^{3+} in soil solutions can be readily calculated from pe (Lindsay 1979). For this reason, and according to pH_p and Eh_p (pe) values registered in soil–peroxide solutions (Table 4), Fe^{3+} was not considered because their concentrations were negligible (Ludwig et al. 2001).

The redox condition could be estimated from pe + pH values, which indicate the redox limits in natural aqueous environments. This parameter ranges between 0 (reduced equilibrium condition, $H_{2(g)}$ 1 atm) and 20.78 (oxidized equilibrium condition, $O_{2(g)}$ 1 atm; Lindsay 1979). The pH_p values ranged from 1.86 to 8.05 and $pe_p + pH_p$ varied from 8.70 to 12.28 (Table 4), indicating highly acidic to basic and oxidized to moderately reduced environments, respectively (Reddy et al. 1995; Devasahayam 2006).

The relationship between the ion activity products (IAP) vs. pH_p for Fe^{2+}, Al^{3+} and SO_4^{2-} solid phases are shown in Fig. 5. The data values from most soil horizons where acid generation was not considerably registered or the soil pHs values were neutral to moderately acidic (e.g., Loyola, Buque, Bustamante and San Julián marshes), Fe^{2+} showed at pH > 5.5 an equilibrium with respect to amorphous oxy-hydroxides of $Fe(OH)_3$ (Fig. 5a). As the soil solutions have been more acidic than pH 5.5, Fe^{2+} and SO_4^{2-} activities showed an equilibrium with respect to soil–$Fe(OH)_3$ and an oversaturation with respect to basic ferric sulfate ($FeOHSO_4$), respectively (Fig. 5a, b). The oxidized soil solutions from Loros and Riacho marshes and from the deeper Cg horizons from Buque profiles have a pH < 4, whereas Fe^{2+} activities were near saturation and oversaturation with respect to goethite (Fig. 5a), while melanterite ($FeSO_4 \cdot 7H_2O$) regulates the dissolved Fe^{2+} and SO_4^{2-} activities at pH < 3 (Fig. 5c). On the other hand, Fe^{2+} and SO_4^{2-} activities at low pHs were oversaturated with respect to basic ferric sulfate (Fig. 5b).

The Al^{3+} activities at pH > 5.5 were oversaturated with respect to gibbsite (San Julián and Loyola high marshes), and from pH more acidic than 5.5, Al^{3+} activities approached equilibrium with respect to $Al(OH)_3$ amorphous (Fig. 5d). While for all samples, Al^{3+} and SO_4^{2-} activities were oversaturated with respect to basic aluminum sulfate (and jurbanite; Fig. 5e).

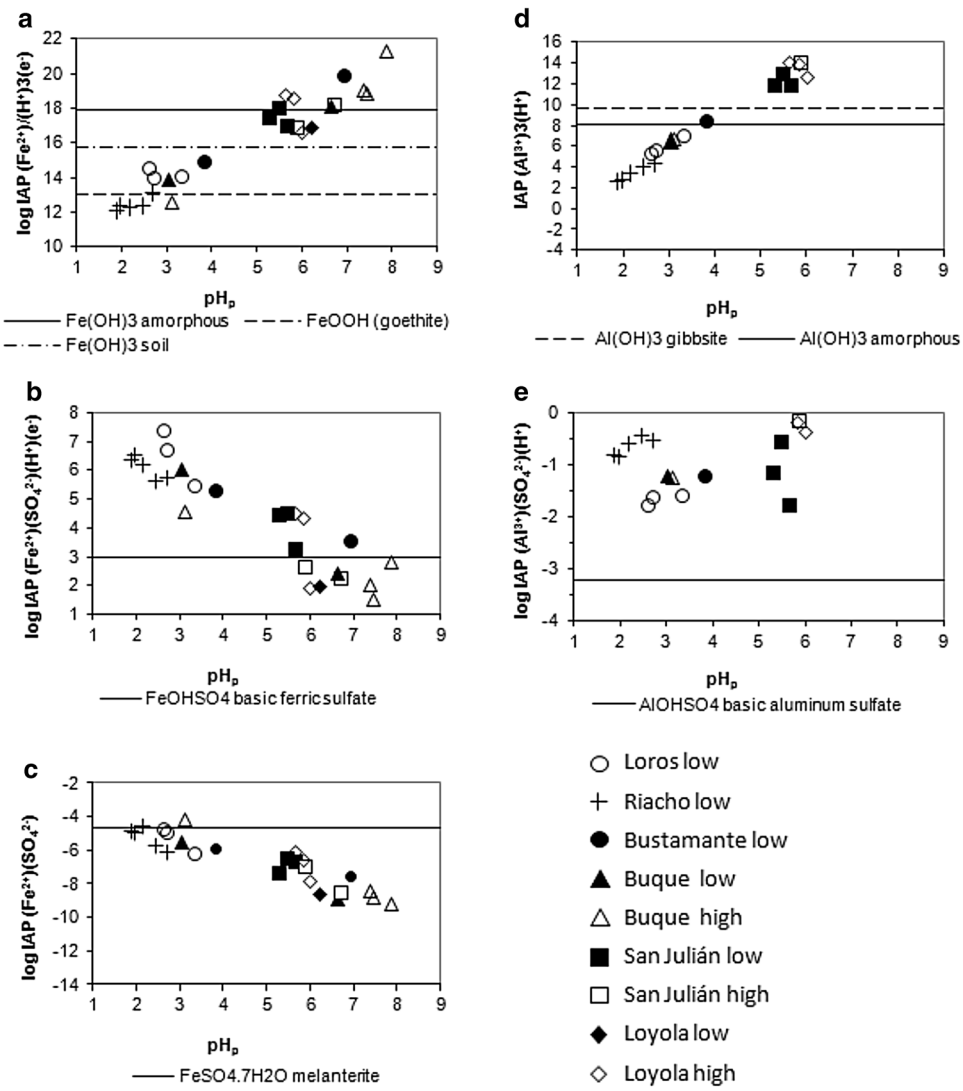

Fig. 5 **a–c** IAP vs. pH_p for Fe^{2+}, and SO_4^{2-}; **d, e** IAP vs. pH_p for Al^{3+}, and SO_4^{2-}

Figure 6 shows SEM-EDS analysis of possible mentioned solid phases after hydrogen peroxide treatment, where relicts of pyrite framboids were not observed by complete oxidation. Figure 6a, b indicates the occurrence of framboids or rounded grains (globules) of iron oxides, while in Fig. 6d, e, a precipitate of Al hydroxysulfate without crystal morphology was observed. Figure 6c–f show the EDS spectrum of the possible oxidation products, where the phosphorus occurrence is also observed.

Discussion

The pyrite occurrence in soils and sediments with predominately sand and silt textures (e.g., Loros and Riacho marshes) could be favorable due to anaerobic bacteria (sulfate reduction) activity in sediments with grain size less than 10 µm in diameter (DeFlaun and Mayer 1983). The spatial variation of pedogenic pyrite seems to have a strong relationship with the *Spartina alterniflora* distribution (Sulfaquent type soils) and the mean annual temperature, or with the combination of both (Table 1).

Sulfate–reducing bacteria (SRB) activity depends on various physicochemical factors, including the supply of sulfates and the amount and type of organic electron donors (Berner 1984). Nie et al. (2009) demonstrated the abundance of SRB which had a close relationship with the decomposition of organic matter produced in *Spartina alterniflora* rhizosphere in late stage (senescent) and therefore promotes both the sulfate reduction rate and the pyrite formation rate.

On the other hand, temperature can affect the population of SRB. While SRB from sediments could be grown well at very low temperatures, the sulfate reduction rates could be greatest at much higher temperatures (Fortin et al. 2000).

Pyrite framboids observed in this study (Fig. 2) were reported with similar characteristics by Wilkin et al. (1996), who were able to calculate that framboids consist of between 102 and 105 discrete pyrite microcrystals. The presence of Si, Al and Na peaks in the energy-dispersive spectra (Fig. 2d) taken from the surface of euhedral pyrite grain could be due to clay minerals caught in the interstices of framboids during their homogenization (Sawlowicz 1993; Merinero et al. 2008). At low temperatures, pyrite growth is usually preceded by the formation of unstable iron monosulfide (mackinawite) followed by greigite (Fe_3S_4). This secondary (pedogenic) formation is related to rapid nucleation from supersaturated solution with respect to FeS_2 (Sawlowicz 1993, 2000).

The inhibition of pyrite oxidation during aerobic incubation could be due to their buffering properties, as carbonate

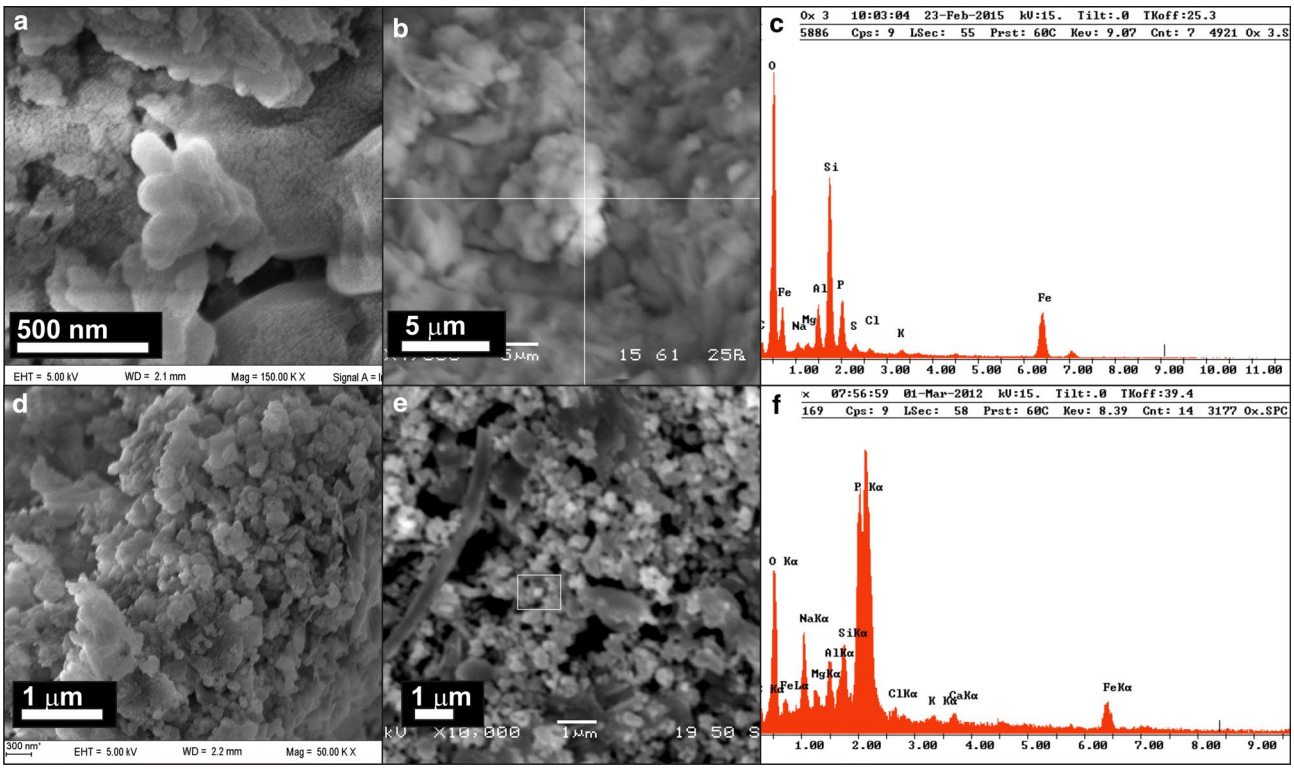

Fig. 6 SEM-EDS analysis after hydrogen with peroxide treatment. **a, b** Possible occurrence of framboids (globules) of goethite–hematite; **c** EDS spectrum from **b** SEM image; **d, e** possible precipitates of Al hydroxysulfate as spherical aggregations of colloids; **f** EDS spectrum from **e** SEM image

contents (shell fragments) and high soil cation-exchange capacity given by clay minerals and/or by organic matter (Table 2). The rapid acidification process by hydrogen peroxide treatment could be producing a breakdown of the buffering mechanism as was expressed by Van Breemen (1982) when a quick oxidation is produced.

In addition, this delay in the rate of oxidation of pyrite can be influenced by the formation of oxy-hydroxide of Fe and Al and silica coatings observed in Fig. 3, as was indicated by Zhang and Evangelou (1996, 1998) in experimental studies. These authors found that at pH higher than 4.0 Fe^{3+} precipitates as $Fe(OH)_3$ forms a coating on the pyrite surface. Similar observations were registered by Otero and Macías (2001) in salt marshes from the Ría de Ortigueira (northwestern of Galicia, autonomous community of Spain) and Osterrieth et al. (2016) in salt marshes from Pampean Plain (Atlantic coast of the Buenos Aires province, Argentina), who identified coatings constituted by amorphous silica and oxy-hydroxides of iron and aluminum, that would prevent pyrite oxidation.

Under hydrogen peroxide treatment, the potential peroxide-oxidizable sulfuric acidity (POSA; Fig. 4) was considered to be an acceptable method to assess potential acidity by oxidation in soils of Patagonian salt marshes, where a negligible contribution from organic acids was identified ($\Delta pH > 0$; Lin et al. 1996; Alsemgeest et al. 2005). The relative variability of POSA at low pH_p values (Fig. 4) may indicate retention of sulfates by hydroxides of Al and Fe present in the sediment residues through the formation of basic Al and Fe minerals (Sullivan et al. 1988a; Lin et al. 1996).

The possible solid phases related with the pH ranges determined in this study (Fig. 5) were also reported by Van Breemen (1973), Nordstrom (1982), Sullivan et al. (1988a, b) and Devasahayam (2006) in acid solutions coming from pyrite oxidation. The observed relationship indicate that in a wide range of pHs of these acidic solutions ($pH < 5.5$), the activities of Fe^{3+} and Al^{3+} are controlled by the basic sulfate solid phase.

The occurrence of framboids or globules of iron oxides shown in Fig. 6 a, b presumably corresponds to goethite–hematite as acidification products (Luther et al. 1982; Schwertmann et al. 2000). On the other hand, the precipitates of Al hydroxysulfate have a lack of any crystal morphology and could occur as spherical aggregations of colloids (Fig. 6d, e; Bigham and Nordstrom 2000; Simón et al. 2005). The presence of other minerals than pyrite into framboids, suggests a physical mechanism of formation (Sawlowicz 2000).

The phosphorus occurrence (Fig. 6c–f) can be related to ortho-phosphate adsorption by aluminum and iron oxide minerals in acid soils (e.g., Goldberg and Sposito 1984; Vepraskas and Faulkner 2001). Phosphorus, like nitrogen and carbon, is considered one of the most important macronutrients in soils. Although phosphorus is often a limiting primary nutrient for plants' growth, in salt marshes it seems to be in excess (DeLaune et al. 1981; Mitsch and Gosselink 2000). For example, phosphorus availability in salt marshes varied between 15 and 25 mg kg^{-1} in northern New England (Theodose and Roths 1999), between 6 and 0.3 mg kg^{-1} in southern Spain (Luque and Arambarri 1983), and between 20 and 6 mg kg^{-1} in northeast China (Xiao et al. 2012). Phosphorous available in superficial horizons of marshes from north-eastern of Chubut province (Península Valdés region) ranged from 50 to 15 mg kg^{-1} (Ríos 2015).

Conclusion

The SEM analysis in selected soil horizons with sulfidic materials reveals the occurrence of framboidal pyrite as the main product of reduction processes.

Aerobic oxidation of sulfuric materials during incubation test would be inhibited by buffering properties, as carbonate contents (shell fragments) and high soil cation-exchange capacity from clay minerals and organic matter. In addition, this delay in the rate of oxidation of pyrite could be influenced by the formation of oxy-hydroxide of Fe and Al and silica coatings. The rapid acidification process by hydrogen peroxide treatment could be producing a breakdown of the buffering mechanism.

The POSA method was considered an acceptable method to assess potential acidity by oxidation in these Patagonian soil marshes. The relationship between ΔpH versus POSA and Eh_p, indicates that acid generation is mainly by pyrite oxidation, with negligible contribution from organic acids. The relative variability of POSA at low pH_p values may indicate retention of sulfates by Al and Fe hydroxides present in the sediment residues, producing the formation of basic aluminum and iron minerals.

These possible oxidized products could be predicted through equilibrium diagrams from soil solution after peroxide treatment. At $pH > 5.5$, Fe^{2+} and Al^{3+} activities show an equilibrium with amorphous oxy-hydroxides of $Fe(OH)_3$ and gibbsite, respectively. As the pH begins to decline below 5.5 (more acidic), Fe^{2+} and Al^{3+} activities show an equilibrium with respect to soil–$Fe(OH)_3$ and $Al(OH)_3$ amorphous, respectively. While for more acidic conditions, the solid phase to predicting both Fe^{2+} and Al^{3+} activities were basic ferric and aluminum sulfates (and jurbanite). The acidic soil solutions with $pH < 3$, Fe^{2+} and SO_4^{2-} activities show equilibrium with goethite (and hematite) and melanterite, respectively. Phosphorus adsorption by aluminum and iron oxide minerals was detected as a consequence of acid generation.

This study constitutes the first survey on potential acid sulfate soils in Patagonian salt marshes, and predicts possible solid phases governing the aluminum and iron

concentrations in soils at low pH. Nevertheless, further research regarding acid generation is needed, principally associated to oxidation of sulfidic materials under natural conditions, to soil buffering processes and to predict solid phase governing, in addition, aluminum and iron, and the other dissolved elements (e.g., heavy metals and arsenic).

Acknowledgements The authors thank Claudia Saín Estela Cortés and Fernando Coronato for their exceptional assistance in laboratory and fieldwork. This research has been funded by the Consejo Nacional de Investigaciones Científicas y Técnicas of Argentina (CONICET, PIP 2014 00190 CO) and Global Environment Fund (GEF- PNUD ARG 02/018 A-B17). The authors are thankful to the comments received from anonymous reviewers and for their suggestions for improving this manuscript.

References

Adam P (1990) Salt marsh ecology. Cambridge University Press, Cambridge

Ahern CR, Ahern MR, Powell B (1998) Guidelines for sampling and analysis of lowland acid sulfate soils (ASS) in Queensland 1998. QASSIT, Department of Natural Resources, Resource Sciences Centre, Indooroopilly, 34 pp

Ahern CR, McElnea AE, Sullivan LA (2004) Acid sulfate soils laboratory methods guidelines. Queensland Department of Natural Resources, Mines and Energy, Indooroopilly, Queensland

Allen JRL (2000) Morphodynamics of Holocene salt marshes: a review sketch from the Atlantic and Southern North Sea coasts of Europe. Quatern Sci Rev 19:1155–1231

Alsemgeest G, Dale P, Alsemgeest D (2005) Evaluating the risk of potential acid sulfate soils and habitat modification for mosquito control (runneling) in coastal salt marshes: comparing methods and managing the risk. Environ Manage 36(1):152–216 **(Australia)**

Berner RA (1984) Sedimentary pyrite formation: an update. Geochim Cosmochim 48:605–615

Bigham JM, Nordstrom DK (2000) Iron and aluminum hydroxysulfates from acid sulfate waters. Rev Miner Geochem 40(1):351–403

Bortolus A, Schwindt E (2007) What would have Darwin written now? Biodivers Conserv 16:337–345

Bortolus A, Schwindt E, Bouza PJ, Idaszkin YL (2009) A characterization of Patagonian salt marshes. Wetlands 29:772–780

Bouza PJ, Sain C, Bortolus A, Ríos I, Idaszkin Y, Cortés E (2008) Geomorfología y Características morfológicas y fisicoquímicas de suelos hidromórficos de marismas patagónicas. XXI Argentinian Soil Science Congress. Extended abstract. Potrero de los Funes, San Luis, Argentina, p 450

Codignotto JO, Kokot RR, Marcomini SC (1993) Desplazamientos verticales y horizontales de la costa Argentina en el Holoceno. Rev Asoc Geol Argent 48(2):125–132

DeLaune RD, Reddy CN, Patrick WH (1981) Accumulation of plant nutrients and heavy metals through sedimentation processes and accretion in a Louisiana salt marsh. Estuaries 4:328–334

Dent D (1986) Acid sulphate soils: a baseline for research and development. International Institute for Land Reclamation and Improvement Publication No. 39, Wageningen

DeFlaun MF, Mayer LM (1983) Relationships between bacteria and grain surfaces in intertidal sediments. Limnol Oceanogr 28(5):873–881

Devasahayam S (2006) Chemistry of acid production in black coal mine washery wastes. Int J Miner Process 79:1–8

Fitzpatrick R, Shand P (2008) Inland acid sulfate soils: overview and conceptual models. In Fitzpatrick R, Shand P (eds) Inland acid sulfate soil systems across Australia, CRC LEME Open File Report No. 249 (Thematic Volume) CRC LEME, Perth pp 6–74

Fortin D, Goulet R, Roy M (2000) Seasonal cycling of Fe and S in a constructed wetland: the role of sulfate-reducing bacteria. Geomicrobiol J 17(3):221–235

Goldberg S, Sposito G (1984) A chemical model of phosphate adsorption by soils: II. Non calcareous soils. Soil Sci Soc Am J 48:779–783

Griffin RA, Jurinak JJ (1973) Estimation of activity coefficients from the electrical conductivity of natural aquatic systems and soil extracts. Soil Sci 116(1):26–30

Haynes RJ (2014) Nature of the belowground ecosystem and Its development during pedogénesis. In: Sparks D (ed) Advances in agronomy, vol 127. Elsevier, Cambridge, pp 43–103

Lin C, Melville MD (1993) Control of soil acidification by fluvial sedimentation in an estuarine floodplain, eastern Australia. Sed Geol 85:271–284

Lin C, Melville MD (1994) Acid sulphate soil–landscape relationships in Pearl River Delta, southern China. Catena 22:105–120

Lin C, Melville MD, Hafer S (1995) Acid sulphate soil–landscape relationships in an undrained, tide-dominated estuarine floodplain, Eastern Australia. Catena 24:177–194

Lin C, Melville MD, White I, Hsu YP (1996) Comparison of three methods for estimation of the reduced-S content in estuarine sediments. Sci Total Environ 87:1–9

Lindsay WL (1979) Chemical equilibria in soils. Wiley, New York, 472 pp

Ludwig B, Prenzel J, Obermann P (2001) Modelling ion composition in seepage water from a column experiment with an open cut coal mine sediment. J Geochem Explor 73:87–95

Luque T, De Arambarri P (1983) Dinámica del fósforo en los suelos de las marismas del río Guadalquivir. Anal Edafol Agrobiol 42:1723–1735

Luther GW, Giblin A, Ryans RA (1982) Pyrite and oxidized iron mineral phases formed from pyrite oxidation in salt marsh and estuarine sediments. Geochim Cosmochim 46:2665–2669

Merinero R, Lunar R, Martínez-Frías J, Somoza L, Díaz-del-Río V (2008) Iron oxyhydroxide and sulphide mineralization in hydrocarbon seep-related carbonate submarine chimneys, Gulf of Cadiz (SW Iberian Peninsula). Mar Pet Geol 25:706–713

Mitsch WJ, Gosselink JG (2000) Wetlands, 3rd edn. Wiley, New York

Nie M, Wang M, Li B (2009) Effects of salt marsh invasion by *Spartina alterniflora* on sulfate-reducing bacteria in the Yangtze River estuary, China. Ecol Eng 35:1804–1808

Nordstrom DK (1982) Aqueous pyrite oxidation and the consequent formation of secondary iron minerals. In: Kittrick JA, Fanning DS, Hossner LR (eds) Acid sulfate weathering. Soil Science Society of America, Madison, pp 37–56

Osterrieth M, Borrelli N, Alvarez MF, Nóbrega GN, Machado W. Ferreira TO (2016) Iron biogeochemistry in Holocene palaeo and actual salt marshes in coastal areas of the Pampean Plain, Argentina. Environ Earth Sci 75:672

Otero XL, Macías F (2001) Caracterización y clasificación de suelos de las marismas de la ría de Ortigueira en relación con su posición fisiográfica y vegetación (Galicia-NO de la Península Ibérica). Edafología 8(3):37–61

Reddy KJ, Wang L, Gloss SP (1995) Potential solid phases controlling dissolved aluminium and iron concentration in acidic soils. In: Date RA et al (eds) Plant and soil interaction at Low pH. Kluwer Academic Publishers, The Netherlands, pp 35–40

Ríos I (2015) Relaciones edafo-geomorfológicas y geo-ecología de plantas vasculares en marismas patagónicas: propiedades

morfológicas, físicas, químicas y biogeoquímicas. Doctoral Thesis, Universidad Nacional de Córdoba, Córdoba, Argentina, p 170
Sawlowicz Z (1993) Pyrite framboids and their development: a new conceptual mechanism. Geol Rundsch 82:148–156
Sawlowicz Z (2000) Framboids: from their origin to application. Pr Mineral 88:1–80
Schoeneberger PJ, Wysocki DA, Benham EC, Soil Survey Staff (2012) Field book for describing and sampling soils, Version 3.0. Natural Resources Conservation Service, National Soil Survey Center, Lincoln
Schwertmann U, Friedl J, Stanjek H, Schulze DG (2000) The effect of Al on Fe oxides. XIX. Formation of Al-substituted hematite from ferrihydrite at 25 °C and pH 4 to 7. Clays Clay Miner 48(2):159–172
SHN (2018) Servicio de Hidrografía Naval Argentina. http://www.hidro.gov.ar/oceanografia/Tmareas/Form_TPSMareas.asp. Accessed 5 May 2018
Simón M, Martín F, García I, Bouza P, Dorronsoro C, Aguilar J (2005) Interaction of limestone grains and acidic solutions from the oxidation of pyrite tailings. Environ Pollut 135:65–72
Soil Survey Staff (1999) Soil taxonomy. A basic system of soil classification for making and interpreting soil surveys; 2nd edition. Agricultural Handbook 436. Natural Resources Conservation Service, USDA, Washington, p 869
Soriano A (1983) Deserts and semi-deserts of Patagonia. In: West NE (ed) Temperate deserts and semi-deserts. Elsevier, Amsterdam, pp 423–460
Sposito G (1989) The chemistry of soils. Oxford University Press, New York, 277 pp
Sposito G, Skipper NT, Sutton R, Park S, Soper AK, Greathouse JA (1999) Surface geochemistry of the clay minerals. Proc Natl Acad Sci USA 96(7):3358–3364
Stevenson FJ (1994) Humus chemistry. genesis, composition, reactions. Wiley, New York
Sullivan P, Yelton J, Reddy KJ (1988a) Solubility relationships of aluminum and iron minerals associated with acid mine drainage. Environ Geol Water Sci 11(3):283–287
Sullivan P, Yelton J, Reddy KJ (1988b) Iron sulfide oxidation and the chemistry of acid generation. Environ Geol Water Sci 11(3):289–295
Sullivan LA, Bush RT, McConchie D, Lancaster D, Haskins PG, Clark MW (1999) Comparison of peroxide-oxidisable sulfur and chromium-reducible sulfur methods for determination of reduced inorganic sulfur in soil. Aust J Soil Res 37:255–265
Theodose TA, Roths JB (1999) Variation in nutrient availability and plant species diversity across forb and graminoid zones of a Northern New England high salt marsh. Plant Ecol 143:219–228
UNEP (1997) United Nations Environment Programme. World atlas of desertification 2nd edition. London, p 182
US Salinity Laboratory Staff (1954) Diagnosis and Improvement of Saline and Alkali Soils, Handbook 60. US Department of Agriculture, Washington, DC, p 160
Van Breemen N (1973) Dissolved aluminum in acid sulfate soils and n mine waters. Soil Sci Soc Am Proc 37:694–697
Van Breemen N (1982) Genesis, morphology and classification of acid sulphate soils in coastal plains. In: Kittrick JA, Fanning DS, Hossner LR (eds) Acid sulphate weathering. Special Publication No. 10. Soil Science Society of America, Madison, pp 95–108
Vepraskas MJ, Faulkner SP (2001) Redox chemistry of hydric soils. In: Richardson JL, Vepraskas MJ (eds) Wetland soils: genesis, hydrology, landscapes, and classification. Lewis Publishers, Washington, D.C, pp 85–105
Vepraskas MJ, Wildings LP, Dress LR (1994) Aquic conditions for soil taxonomy: concepts, soil morphology and micromorphology. In: Ringrose-Voace, Humphreys GS (ed) Soil micromorphology: studies in management and genesis, development in soil science 22. Elsevier, Amsterdam, pp 117–131
White I, Melville MD, Wilson BP, Sammut J (1997) Reducing acidic discharges from coastal wetlands in eastern Australia. Wetlands Ecol Manag 5:55–72
Wilkin RT, Barnes HL, Brantley SL (1996) The size distribution of framboidal pyrite in modern sediments: an indicator of redox conditions. Geochim Cosmochim 60:3897–3912
Xiao R, Bai J, Gao H, Huang L, Deng W (2012) Spatial distribution of phosphorus in marsh soils of a typical land/inland water ecotone along a hydrological gradient. Catena 98:96–103
Yagui R, Ferreira ME, Pessôa da Cruz MC, Barbosa JC (2003) Organic matter fractions and soil fertility under the influence of liming, vermicompost and cattle manure. Sci Agric 60(3):549–557
Zhang YL, Evangelou VP (1996) Influence of iron oxide forming conditions on pyrite oxidation. Soil Sci 161:852–864
Zhang YL, Evangelou VP (1998) Formation of ferric hydroxide-silica coatings on pyrite and its oxidation behavior. Soil Sci 163:53–62